Received: 26 November 2018 | Revised: 23 July 2019 | Accepted: 25 July 2019

DOI: 10.1002/mrm.27951

RAPID COMMUNICATION

Magnetic Resonance in Medicine

In vivo potassium MRI of the human heart

Daniel Wenz[1] | **Armin Michael Nagel**[2,3,4] | **Johanna Lott**[4] | **Andre Kuehne**[5] | **Sebastian Christian Niesporek**[4] | **Thoralf Niendorf**[1,5]

[1]Berlin Ultrahigh Field Facility (B.U.F.F.), Max Delbrueck Center for Molecular Medicine in the Helmholtz Association, Berlin, Germany

[2]Institute of Radiology, University Hospital Erlangen, Friedrich-Alexander-Universität Erlangen-Nürnberg (FAU), Erlangen, Germany

[3]Institute of Medical Physics, University of Erlangen, Friedrich-Alexander-Universität Erlangen-Nürnberg (FAU), Erlangen, Germany

[4]Division of Medical Physics in Radiology, German Cancer Research Centre (DKFZ), Heidelberg, Germany

[5]MRI.TOOLS GmbH, Berlin, Germany

Correspondence
Thoralf Niendorf, Berlin Ultrahigh Field Facility (B.U.F.F.), Max-Delbrueck-Center for Molecular Medicine, Robert-Roessle-Strasse 10, 13125 Berlin, Germany.
Email: thoralf.niendorf@mdc-berlin.de

Funding information
Helmholtz Alliance iMED, the Helmholtz Initiative on Personalized Medicine.

Purpose: Potassium ions (K^+) play a critical role in cardiac electrophysiology, and changes in their concentration reflect pathophysiological processes related to cardiovascular diseases. Here, we investigated the feasibility of in vivo ^{39}K MRI of the human heart. To achieve this, we developed, evaluated, and applied a $^{39}K/^{1}H$ RF coil, which is tailored for ^{39}K MRI of human heart at 7.0T.

Methods: The performance of the $^{39}K/^{1}H$ RF coil was evaluated by electromagnetic field and specific absorption ratio simulations using 2 (male/female) human voxel models. The RF coil was evaluated at the bench and applied in an in vivo proof-of-principle study involving 7 healthy volunteers. The experiments were performed using a 7.0T whole-body MR system in conjunction with a 3D density-adapted projection reconstruction imaging technique.

Results: For in vivo ^{39}K MRI of the human heart, a nominal spatial resolution of 14.5 × 14.5 × 14.5 mm^3 within a total scan time of 30 min was achieved. The average SNR within the heart was 9.6 ± 2.4.

Conclusion: This work validates the design of a $^{39}K/^{1}H$ RF coil for cardiac MR at 7.0T and demonstrates for the first time in vivo the feasibility of ^{39}K MRI of the human heart.

KEYWORDS
cardiac imaging, heart, MRI, potassium MRI, radio frequency coil, ultrahigh field MRI

1 | INTRODUCTION

Potassium ion (K^+) channels are one of the largest and most functionally diverse families of ion-channel proteins in the human genome.[1] Sodium/potassium pumps (Na^+/K^+-ATPase) play crucial roles in human physiology and metabolism,[2] and therefore ^{39}K MRI has the potential to provide unique insights into the activity of this system. Potassium plays a key role in cardiac electrophysiology.[3,4] Increased extracellular K^+ concentration following ischemia can induce ventricular arrhythmia.[5,6] Conversely, decreased tissue K^+ has been shown to lead to irreversible injury to cardiomyocytes.[7] Potassium is vasoactive and is important in regulating smooth muscle tone and blood flow.[8] Altered smooth muscle

K^+ channel function has been implicated in several pathological conditions.

MRI provides a means for probing ^{39}K in vivo, but this remains challenging because of sensitivity constraints. The NMR sensitivity of ^{39}K is ~180 times lower than that of ^{23}Na, and 2000 times lower than that of ^{1}H. The SNR gain afforded by ultrahigh field MRI (UHF-MR) leads to the possibility to investigate ^{39}K with a diagnostically meaningful spatial resolution and with total acquisition times that are potentially feasible for human application. In contrast to current laboratory diagnostics that can only measure extracellular potassium concentration, ^{39}K MRI is sensitive to changes in the total tissue potassium concentration (TPC). Since ~98% of potassium ions are located in the intracellular space, ^{39}K MRI detects K^+ almost exclusively from the intracellular space. Therefore, ^{39}K MRI has the potential to detect changes in the intracellular volume fraction and the intracellular K^+ concentration that cannot be revealed by the diagnostic methods currently used.

The aim of this study was to use the sensitivity gain of UHF-MR to demonstrate the feasibility of ^{39}K MRI of the human heart, by designing and constructing a $^{39}K/^{1}H$ RF coil customized for cardiac MRI at 7.0T. Here we provide the first data on ^{39}K MRI of the human heart acquired in vivo.

2 | METHODS

2.1 | RF coil design

The RF coil design is comprised of two separate coil sets operating at f_{39K} = 13.9 MHz and f_{1H} = 297.2 MHz (Figure 1). It consists of an anterior and a posterior module, with the former being curved to conform to an average human torso. Each module is composed of one large loop element (270 × 280 mm^2) tuned to f_{39K} and two concentric smaller loop elements (220 × 200 mm^2) tuned to f_{1H}. The ^{39}K loop elements are built of copper tube (outer diameter = 4 mm, wall thickness = 1 mm) and connected as a Helmholtz coil. The four ^{1}H loop elements (conductor width = 10 mm) were manufactured from 36 μm copper on a 0.5 mm FR-4 substrate. Constructive interference in the heart was achieved via static transmit field (B_1^+) shimming using appropriate phase delay cables connected to the ^{1}H channels. The adjacent ^{1}H loop elements share a common conductor and were decoupled capacitively using a trimmer capacitor. Each channel of the four-channel ^{1}H array was equipped with two cable traps tuned to f_{1H} and f_{39K}. For the ^{39}K Helmholtz coil, one cable trap tuned to f_{1H}, was used ($\lambda_{39K} \approx 22$ m). The size of the ^{39}K loop elements was chosen to provide acceptable signal uniformity in the region of interest (ROI), sufficient coverage of the heart and to minimize coupling with the ^{39}K coil. No additional circuits were used to decouple ^{1}H from ^{39}K, because both resonant frequencies are sufficiently distant from each other. The placement of the proposed $^{39}K/^{1}H$ RF coil is slightly off the long axis of the torso, which helps to keep the connection between Helmholtz loops as short as possible. The coil casing, shown in Figure 2, was designed by using Autodesk Inventor Professional 2017 (Autodesk Inc., San Rafael, CA) and constructed from acrylonitrile butadiene styrene (ABS) material using a 3D printer (BST 1200es; Dimension Inc., Eden Prairie, MN).

2.2 | Numeric EMF simulations

Electromagnetic field (EMF) simulations were performed to examine the transmit field (B_1^+) distribution at both resonance frequencies (f_{39K} and f_{1H}). This was particularly important for f_{1H} because of the short wavelength in tissue at 297.2 MHz, which might induce B_1^+ destructive interferences in the cardiac ROI, which can be offset by static B_1^+ shimming. Specific absorption rate (SAR) simulations for both resonance frequencies were conducted to meet the requirements of the International Electrotechnical Commission (IEC) guidelines IEC 60601-2-33 Ed.3 for local transmit coils (first level controlled: local SAR = 20 W/kg for 6 min averaging time).[9] SAR simulations do not require detailed information about the RF pulse shape and pulse sequence used, because the RF input power in the simulations is pulse-normalized and time-averaged. This approach provides the value of the conversion factor (the k-factor) that specifies the local SAR produced per 1 W transmitted RF power. The k-factor must be defined for a given RF coil in a configuration file, which is required by the MR systems software. During an in vivo acquisition, the average RF power for a given RF pulse is multiplied by the k-factor value. This approach enables the RF pulse sequence to be used and is directly linked to the local SAR simulations. Other tests are performed by the RF power monitoring system (that is a part of the MR scanner) at various stages of the RF chain, to ensure RF safety. These include, for example, RF power calibration units (prospective and real-time) that provide the user-defined voltage RMS value (V_{RMS}) at the RF coil plug.

For the EMF and SAR simulations, we used the Finite Integration Technique (FIT) of CST Studio Suite 2015 (CST AG, Darmstadt, Germany) with the human voxel models Duke (male) and Ella (female) from the Virtual Family.[10] The electrical properties of all tissues were defined according to the IT'IS database (IT'IS, Zurich Switzerland).[11] The scattering parameter matrix (S-parameter matrix) results obtained from the EMF simulations were exported from the CST Studio Suite into Advanced Design System (ADS) (Keysight EEsof EDA, Santa Rosa, CA) for tuning and matching. The S-parameter matrix shows how RF power is distributed in a multi-port network. For the purposes of this work, it was

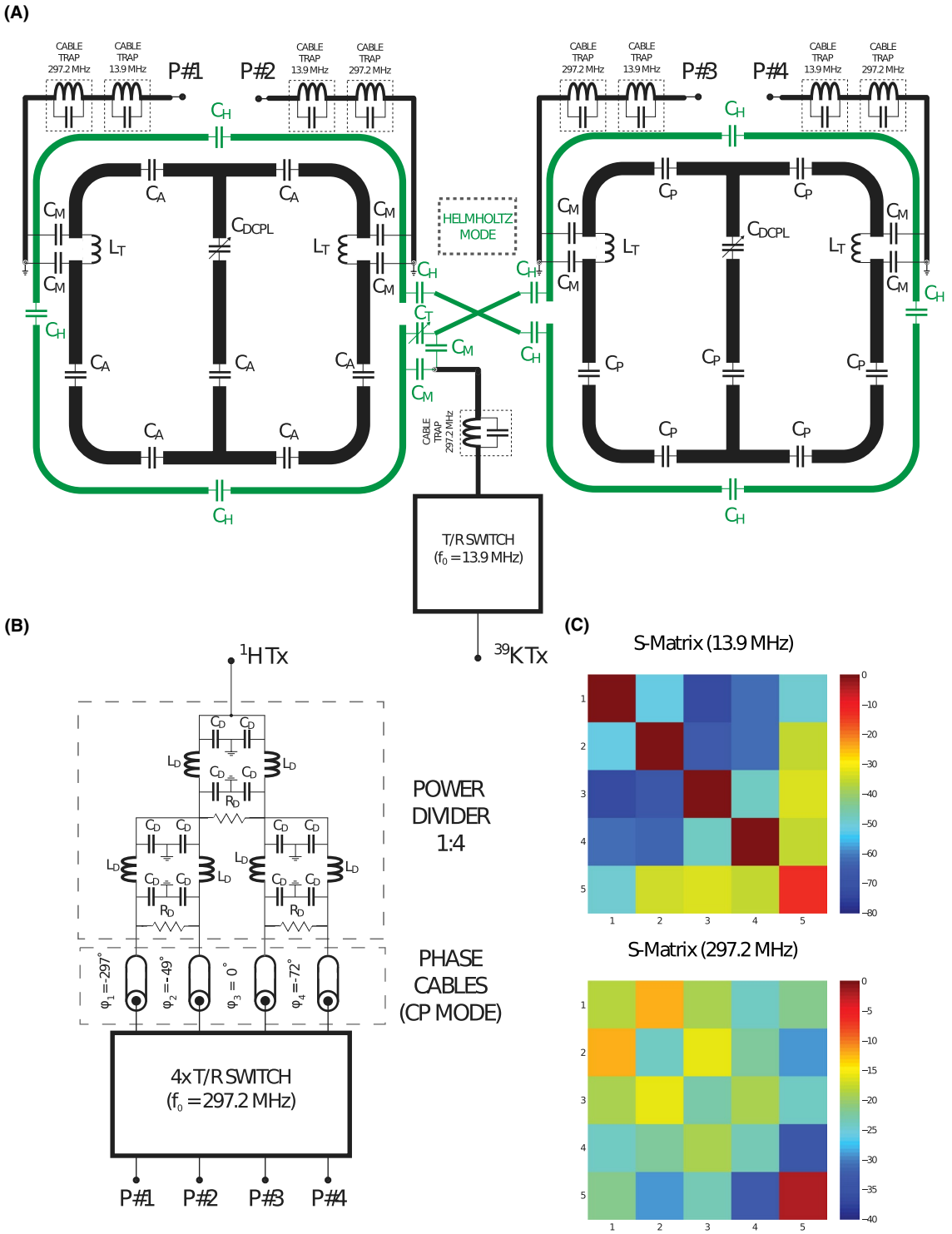

FIGURE 1 (A) Schematic of the proposed ^{39}K/^{1}H RF coil. The pair of ^{39}K Helmholtz loops are highlighted in green. The 4-channel ^{1}H transceiver array is in black. (B) The RF signal was divided by using Wilkinson splitter and connected to the T/R switch box through phase cables that supported CP mode. (C) S-Parameter matrix averaged over 8 volunteers is shown for both resonant frequencies (13.9 and 297.2 MHz). Coupling between both coils was weaker at the lower frequency ($S_{15} = -49.5$ dB, $S_{25} = -34.6$ dB, $S_{35} = -33.4$ dB, $S_{45} = -35.3$ dB) than at the higher frequency ($S_{15} = -21.8$ dB, $S_{25} = -29.3$ dB, $S_{35} = -23.4$ dB, $S_{45} = -33.0$ dB). Averaged values for reflection coefficients (297.2 MHz) were: -18.2 dB for S_{11}, -24.2 dB for S_{22}, -22.8 dB for S_{33}, and -23.7 dB for S_{44}. The capacitive decoupling for the anterior part of the RF coil yielded $S_{12} = -12.5$ dB, and $S_{23} = -16.0$ dB for the posterior part

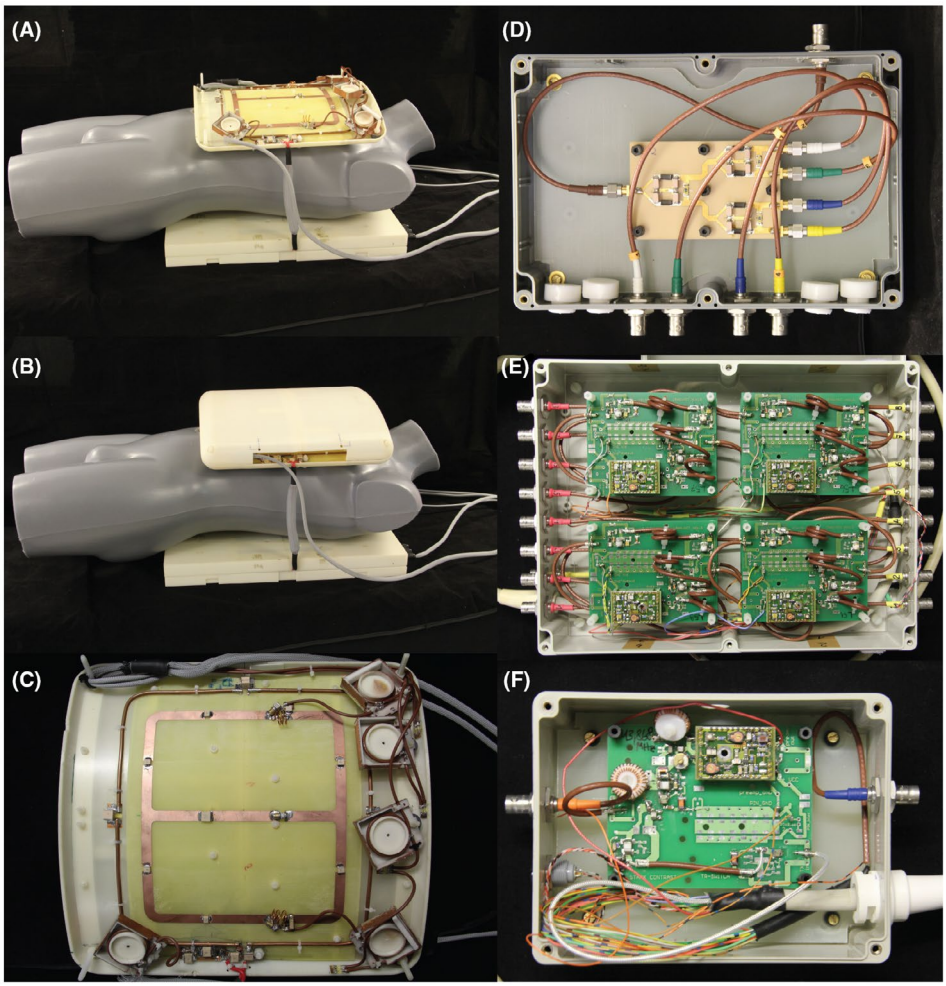

FIGURE 2 The proposed $^{39}K/^{1}H$ RF coil placed on a mannequin without (A) and with (B) upper part of the casing along with a zoomed view (C) at the anterior module of the coil. (D) A 1:4 power divider ($f_0 = 297.2$ MHz), an interface box (E) containing 8 T/R switches (4 of which were used in our study; $f_0 = 297.2$ MHz) and an interface box (F) containing 1 T/R switch ($f_0 = 13.9$ MHz) were used to connect the $^{39}K/^{1}H$ RF coil with the scanner

sufficient to highlight that in an ideal case all of the entries of an n-element S-parameter matrix that describes an n-channel RF coil would approach zero (on a linear scale). The diagonal elements of such a matrix inform how well a given element of an RF coil is matched to the load, while non-diagonal ones inform about the electromagnetic coupling between specific elements of the coil.

The final circuit designed in ADS was reproduced in the schematic view in CST for alternating current (AC) simulation and field combination. This set-up was used to calculate the B_1^+ of the $^{39}K/^{1}H$ RF coil and SAR distribution in the human voxel models Duke and Ella. The input power for the in vivo experiments was adjusted to meet the regulations provided by the IEC guidelines.

We provided a circularly polarized (CP) mode for 4-channel ^{1}H array within the region of interest. To achieve this, the EMF simulations, which involved the human voxel model Duke, were used. The B_1^+ fields generated by each channel of the ^{1}H 4-channel array (i.e., with only one channel transmitting at a time) were analyzed, and a transversal slice placed across the center of the heart in the Duke model was used to read out the B_1^+ phase corresponding to each. The phases provided by all four channels of the ^{1}H array were directly used in a combined simulation involving all of the channels. The phases were normalized to keep the real cable lengths as short as possible. The same phases were used to generate a CP mode within the heart of the human voxel model Ella.

2.3 | Bench evaluation

Bench measurements were performed using an 8-channel vector network analyzer (ZVT 8; Rohde & Schwarz, Memmingen, Germany). Full sets of S-parameters were measured for various loading conditions, including 8 volunteers (BMI ranging from 18.9–28.5 kg/m^2). Each subject had provided a written consent before any measurement was conducted. S-parameter matrices were measured, exported

from the network analyzer and processed in MATLAB (The MathWorks, Natick, MA). The quality factor (Q) of the coil was evaluated for two cases: unloaded (Q_{UL}) and when the coil was loaded with a torso phantom (Q_L).

2.4 | Phantom experiments

A torso phantom was designed and built to evaluate RF coil performance at both resonant frequencies. The phantom (MRI.TOOLS GmbH, Berlin, Germany, volume ≈ 35 l; length = 50 cm; permittivity $\varepsilon_r = 81$, conductivity $\sigma = 0.81$ S/m) was filled with an aqueous solution of K_2HPO_4 ($[K^+]$ = 80 mmol/L), which is significantly less conductive than KCl. This approach enabled the use of a greater absolute amount of K^+ ions, while maintaining the conductivity similar to that of muscle tissue at 297.2 MHz ($\sigma = 0.77$ S/m). The electrical properties of the aqueous solution were constant over the frequency range (10–300 MHz).

2.5 | MR hardware

Initial phantom and human studies ($N = 1$) were conducted on a 7.0T whole-body MR system (Magnetom, Siemens Healthineers, Erlangen, Germany), equipped with a gradient system supporting dG/dt_{max} = 170 mT/m/ms, G_{max} = 38 mT/m. The MR system is provided with a broadband 8 kW RF power amplifier (RFPA) (Stolberg HF-Technik AG, Stolberg-Vicht, Germany) that was used for all of the experiments involving nuclei other than ^{1}H that are supported by the system (^{23}Na, ^{7}Li, etc.). ^{1}H MRI was performed using another narrowband 8 kW RFPA. Further in vivo experiments ($N = 6$), were conducted using another 7.0T whole-body MR system (Terra, Siemens Healthineers) that supports ^{39}K MRI. This MR system is equipped with a gradient system supporting dG/dt_{max} = 200 mT/m/ms, G_{max} = 80 mT/m.

The multipurpose interface boxes used to connect the coils to the scanner (Figure 2) consist of four transmit/receive switches for 297.2 MHz and one transmit/receive switch for 13.9 MHz along with integrated low-noise preamplifiers for each of the resonant frequencies (Stark Contrast, Erlangen, Germany).

2.6 | In vivo feasibility study

The in vivo feasibility study was carried out in compliance with institutional guidelines and was approved by the Ethical Review Board of the Friedrich-Alexander University Erlangen-Nuremberg. Each subject provided a written consent before any measurement was conducted. Proof-of-principle in vivo MRI was performed in 7 healthy subjects (4 male, 2 female; average BMI = 24.1 kg/m^2, average age = 34 y).

Potassium imaging was conducted with a 3D density adapted projection reconstruction (3D-DAPR)[12] imaging technique (TR = 30 ms; TE = 0.7 ms; number of projections = 20,000; read-out duration = 5 ms; maximum gradient amplitude = 11.95 mT/m, slew rate = 170 T/(m × s), beginning of the density-adapted part at t0 = 0.5 ms, rectangular pulse duration = 1 ms; radial samples = 64; dwell time = 78.1 μs; nominal isotropic resolution = (14.5 × 14.5 × 14.5) mm^3. The acquisition time was 30 min. The RF coil and receiver chain did not support simultaneous ^{39}K/^{1}H imaging.

^{39}K relaxation times of myocardium and blood are unknown. However, it has been demonstrated at 7.0T that the T_1 relaxation time in thigh muscle tissue is 5.7 ± 0.4 ms.[13] Assuming similar or even slightly longer T_1 relaxation times for myocardium, we did not expect saturation effects in myocardium (TR > 5 T_1). Only the ^{39}K signal originating from the blood might have been partially saturated, because longer relaxation times in red blood cells (T_1 = 19.3 ms) have been previously reported.[14] Given the short transverse relaxation times of thigh muscle tissue (T^*_{2fast} = 1.5 ms; T^*_{2slow} = 9.7 ms),[15] we also expected short relaxation times for myocardium. Therefore, to limit the relaxation during the excitation pulse, we did not increase the pulse duration (1 ms). Given the short relaxation times, the use of an UTE sequence was considered to be mandatory for ^{39}K MRI. In addition, a density-adapted readout can be used to improve SNR compared to a conventional UTE sequence with trapezoidal gradients. Therefore, we used the pulse sequence that we optimized for ^{39}K MRI of the human brain,[13] although the flip angle could not be determined. During the calibration procedure, an approximately linear increase of the signal intensity with pulse voltage was found and a reliable sinusoidal fit of the required pulse voltage was not possible. Therefore, it is expected that the flip angle is lower than 60°. The RF power was maximized given the coil specifications (i.e., limited only by SAR). The image reconstruction was performed using non-uniform fast Fourier transform (NUFFT).

For ^{1}H CINE imaging of the heart 2 (2CV), 3 (3CV), 4 chamber (4CV), and short axis (SAX) views were acquired using breath-hold 2D CINE FLASH (TE = 2.67 ms, TR = 5.66 ms, matrix size = 256 × 256, FOV) = (360 × 291) mm^2, in-plane spatial resolution = (1.4 × 1.4) mm^2, slice thickness = 4.0 mm, flip angle = 32°, receiver bandwidth = 444 Hz/pixel, acquisition time = 12 s.

3 | RESULTS

3.1 | RF coil performance

The S-parameter matrices were measured at both resonant frequencies and averaged over 8 volunteers (Figure 1). Before all measurements, the proposed RF coil was placed on the cylindrical phantom and tuned and matched. The average reflection coefficient S_{55} for the ^{39}K coil was −13.5 dB. Coupling between the ^{39}K coil and the 4-channel ^{1}H array was negligible, at 13.9 MHz (all below −33.4 dB). Coupling

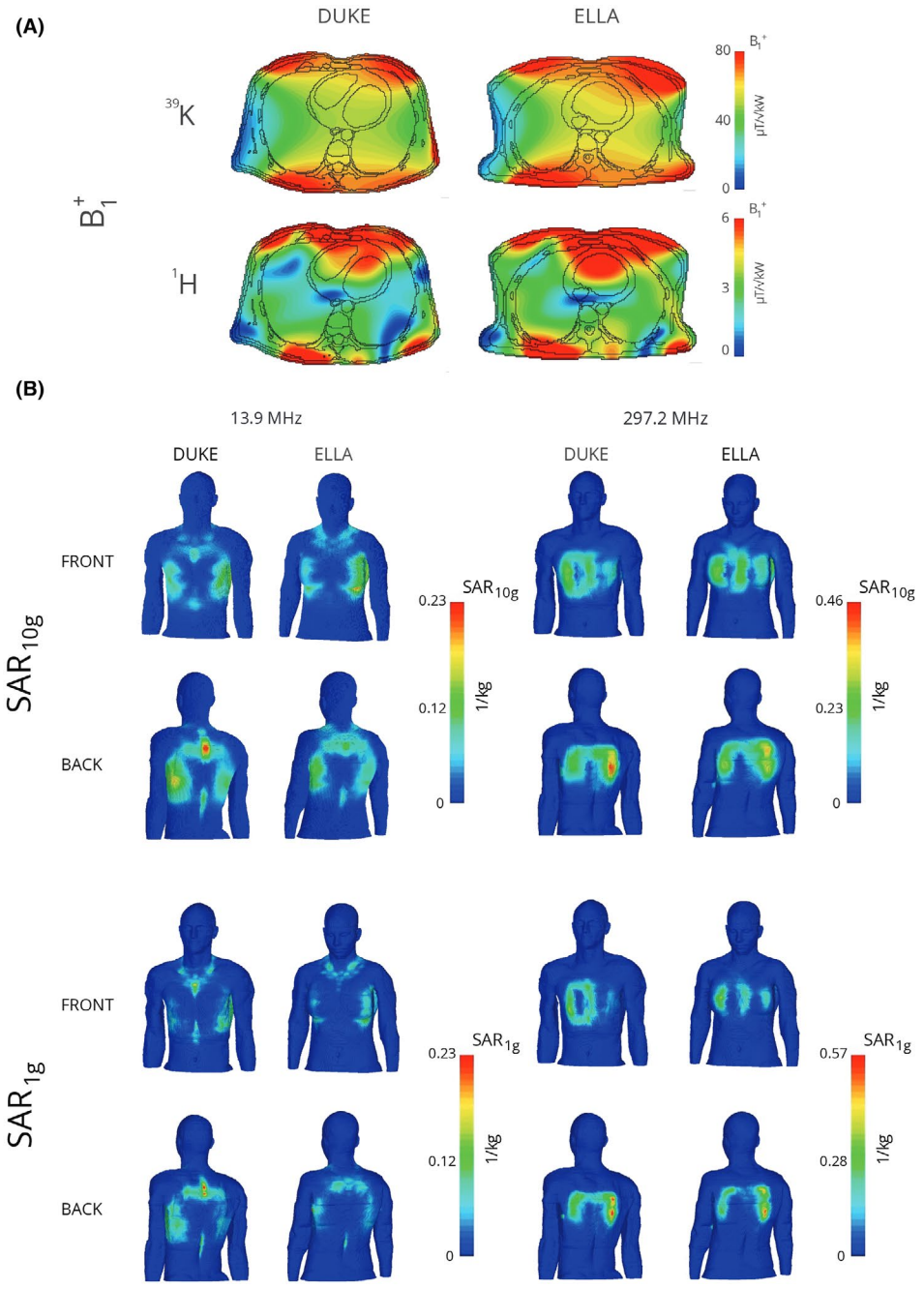

FIGURE 3 (A) Transmit field (B_1^+) distribution for an axial cardiac plane of the human voxel models Duke (left) and Ella (right), for the resonant frequencies: 13.9 MHz (^{39}K, top row) and 297.2 MHz (^{1}H, bottom row). The outcomes were normalized to the square root of kilowatt (average input power = 1 kW what results in V_{RMS} = 223 V). The black contours represent the anatomic features including the heart which is localized off-center. Based on qualitative assessment, the ^{39}K Helmholtz loops provide good B_1^+ homogeneity. The CP mode applied for the 4-channel ^{1}H array provides fairly constructive B_1^+ interference for whole heart coverage. (B) SAR_{10g} and SAR_{1g} distribution for both resonant frequencies (13.9 MHz and 297.2 MHz) for both human voxel models Duke and Ella shown in 3D. SAR simulations were performed for input power of 1 W. SAR_{10g} distributions were scaled to the maximum SAR_{10g} value for Ella (0.23 W/kg at 13.9 MHz) to highlight good qualitative and quantitative (0.21 W/kg maximum SAR_{10g} value for Duke) agreement between SAR distributions for both human voxel models. The maximum SAR_{10g} values obtained at 297.2 MHz were scaled to the maximum SAR_{10g} for Duke (0.46 W/kg at 297.2 MHz) which was slightly higher than for Ella (0.37 W/kg). A hotspot on the back of Duke at 13.9 MHz results from close vicinity of vertebral disc with respect to the conductive element of the RF coil. In case of Ella, the vertebral disc is located further away from the coil. SAR values averaged over 1 g (SAR_{1g}) are shown in the lower part of the figure. Although there was no change observed for f_{39K}, there was an increase in SAR_{1g} with respect to SAR_{10g} for f_{1H}. Local SAR_{1g} maxima were found to be 0.57 W/kg for Duke and 0.55 W/kg for Ella

at 297.2 MHz was within an acceptable range, between −21.8 dB and −33.0 dB. The phantom measurements yielded Q_{UL} = 141, Q_L = 27, and the Q_{UL}/Q_L = 5.2 for the ^{39}K Helmholtz coil. The tuning and matching procedure was conducted at the bench. There was no appreciable frequency shift when the coil was loaded with a torso phantom and placed inside the bore of the magnet. The following changes in matching were observed: S_{11}: from −28.7 to −27.0 dB, S_{22} from −28.3 to −30.2 dB, S_{33} from −21.9 to −23.0 dB, S44 from −27.6 to −26.7 dB, and S_{55} from −22.3 to −25.6 dB).

3.2 | EMF and SAR simulations

To achieve CP mode within the ROI in the human voxel model Duke, the phases were set as follows: channel 1: −297°, channel 2: −72°, channel 3: 0°, channel 4: −49°. The same phase settings were applied for the human voxel Ella. The B_1^+ distribution for ^{39}K was very similar for both human voxel models (Figure 3A). The results for ^{1}H show that despite obvious anatomic differences, the CP mode can be used to produce acceptable in vivo anatomic reference images. Local SAR values averaged over 10 g (SAR_{10g}) were derived from the EMF simulations for both frequencies using the human voxel models Duke and Ella for an input power of 1 W (Figure 3B). Local SAR_{10g} maxima were found to be 0.21 W/kg for Duke and 0.23 W/kg for Ella for f_{39K} and 0.46 W/kg for Duke and 0.37 W/kg for Ella for f_{1H}. Additional EMF simulations also provided local SAR values averaged over 1 g (SAR_{1g}) (Figure 3B). While there was no change observed for f_{39K}, there was an increase in SAR_{1g} with respect to SAR_{10g} for f_{1H}. Local SAR_{1g} maxima were found to be 0.57 W/kg for Duke and 0.55 W/kg for Ella. The ^{39}K RF coil was driven with time-averaged forward power limited to 100 W to stay below the 20 W/kg limit (first level controlled SAR) set by the IEC guidelines. The time-averaged forward power for ^{1}H 4-channel array was limited to 40 W.

3.3 | In vivo feasibility study

Following evaluation experiments in the torso phantom (Figures 4 and 5), we went on to conduct a feasibility study in vivo, which yielded ^{39}K images and ^{1}H images of the human heart (Figures 6 and 7). For ^{39}K MRI of the heart, a nominal isotropic spatial resolution of (14.5 × 14.5 × 14.5) mm^3 was achieved within 30 min of scan time. The in vivo images showed 3 regions with high ^{39}K signal intensity. The SNR within the heart was estimated by dividing the signal in the ROI by the SD of the signal in the background. The average SNR (mean/SD) was SNR = 9.6 ± 2.4 (Figure 7; for male volunteers: MV1 = 9.2, MV2 = 8.7, MV3 = 8.7, MV4 = 6.3; for female volunteers: FV1 = 13.1, FV2 = 11.6). Based on information obtained from anatomical reference images and data from the literature,[7,13] these regions correspond to the heart and the muscles of the thorax (anterior and posterior part). No significant B_1^+ destructive interferences were observed for the cardiac area used for ^{1}H MR.

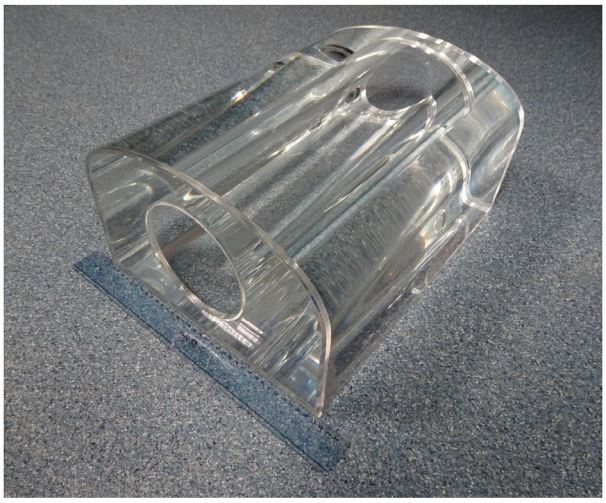

FIGURE 4 Torso phantom (MRI.TOOLS GmbH, Berlin, Germany, volume ≈ 35 l; length = 50 cm; permittivity ε_r = 81, conductivity σ = 0.81 S/m) that was filled with an aqueous solution of K_2HPO_4 ([K^+] = 80 mmol/L)

4 | DISCUSSION AND CONCLUSIONS

In this work, we demonstrate the feasibility of in vivo ^{39}K MRI of human heart at 7.0T. These in vivo experiments revealed three regions in the ^{39}K images with high signal intensity. Based on prior anatomic information, these regions correspond to the heart and thoracic muscles (anterior and posterior parts). This is in agreement with the literature and previous studies that showed substantial K^+ content in muscle tissue.[13] Note that the blood ^{39}K signal was barely distinguishable from the myocardial signal (Figure 6). The blood is mainly composed of blood serum and erythrocytes; although there is very little K^+ in blood serum ([K^+] ≈ 5 mM), potassium cations are nevertheless present within erythrocytes.[16] Assuming that erythrocytes represent 45% of blood volume, the total [K^+] in the blood is then [K^+] ≈ 45 mM. This erythrocyte compartment contributes to the overall ^{39}K signal being detected.

The theoretical basis for sodium and potassium MRI of the human heart at 1.5T was originally provided by simulations.[5] This first report suggested that ^{39}K MRI of the heart with isotropic spatial resolution of 13 mm^3 and a scan time of 30 min could be considered "clinically useful." These previous simulations concluded that the sensitivity that could be obtained at 1.5T was not sufficient to achieve this goal, and an 8-fold increase in SNR would be required. In the current

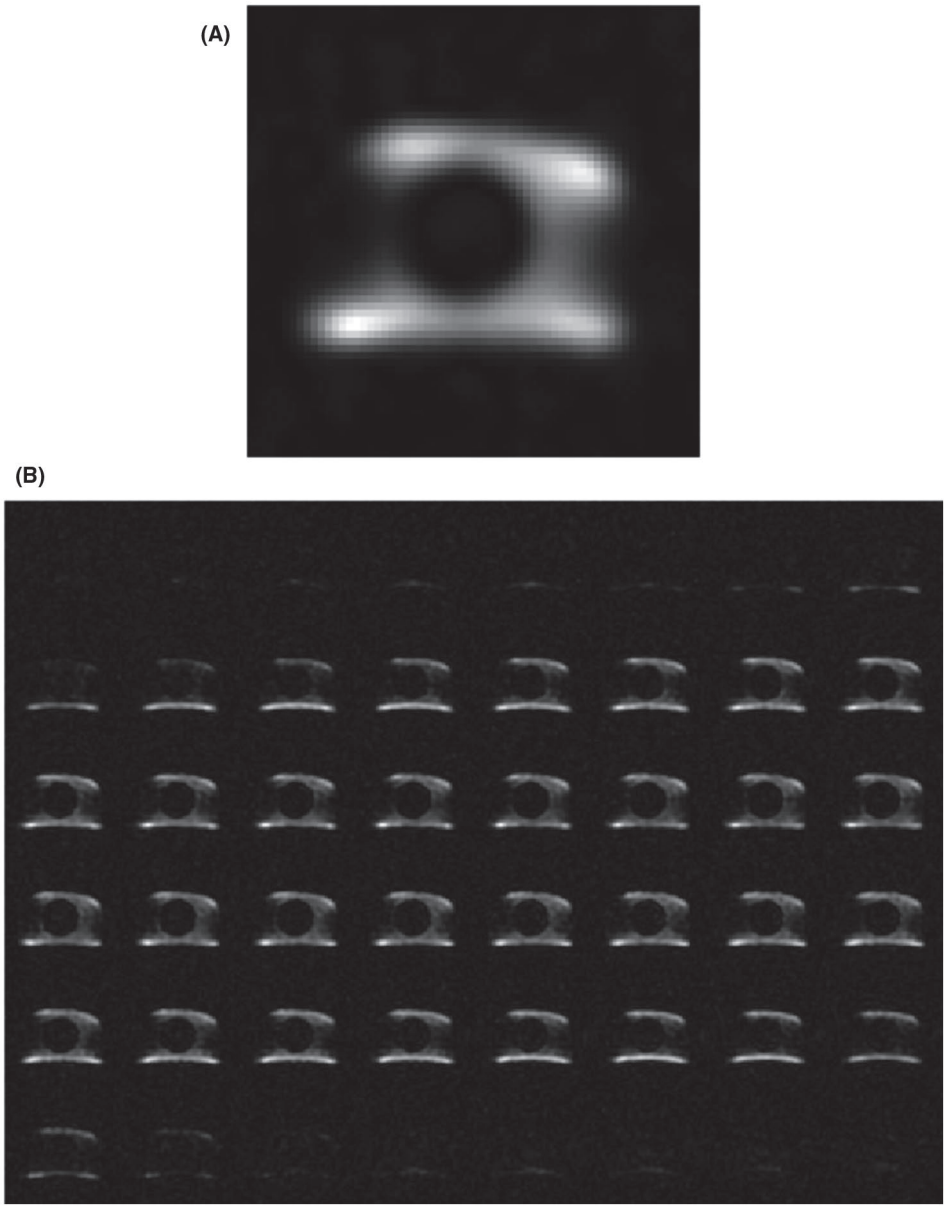

FIGURE 5 (A) An axial slice through the center of the phantom obtained using 3D-DAPR imaging technique: TR/TE = 300/1.5 ms, number of averages = 5, number of projections = 12000, readout time = 10 ms transmit voltage = 223 V, FOV = 479 × 479 mm^2, nominal spatial resolution = 15 mm^3; Gaussian filter has been applied. (B) Full set of axial slices obtained using the same protocol as in (A), without using Gaussian filter

study we were able to approach this level with our experiments at 7.0T, by achieving isotropic spatial resolution of 14.5 mm^3 with a scan time of 30 min.

The configuration of the $^{39}K/^{1}H$ RF coil proposed herein supports in vivo ^{39}K and ^{1}H imaging of the human heart at 7.0T. The $^{39}K/^{1}H$ RF coil is light-weight, ensures patient comfort, and can be applied to an average human torso. Driving the ^{39}K loop elements in Helmholtz mode provides good B_1^+ field homogeneity, as demonstrated in our EMF simulations and in our in vivo measurements. The 4-channel ^{1}H transceiver array yielded anatomic images of sufficient quality to serve as a reference for the ^{39}K images.

In the proposed RF coil, the loop elements for both resonant frequencies are placed in close proximity to the target anatomy and ROI used for imaging. This is advantageous for transmit efficiency and is particularly useful for receive sensitivity of imaging experiments involving ^{39}K ($\gamma_{1H}/\gamma_{39K} \cong 21$). An alternative to this design might be an elliptical (or Cassini oval-shaped)[17,18] birdcage design. However, to achieve a similar transmit efficiency as shown in the current study, such a design would have to be a very close-fitting volume coil.

We did not use multiple turns for our $^{39}K/^{1}H$ RF coil as the Q_{UL}/Q_L ratio indicated that the losses were sample-dominated. This is not surprising for a close-fitting coil even at

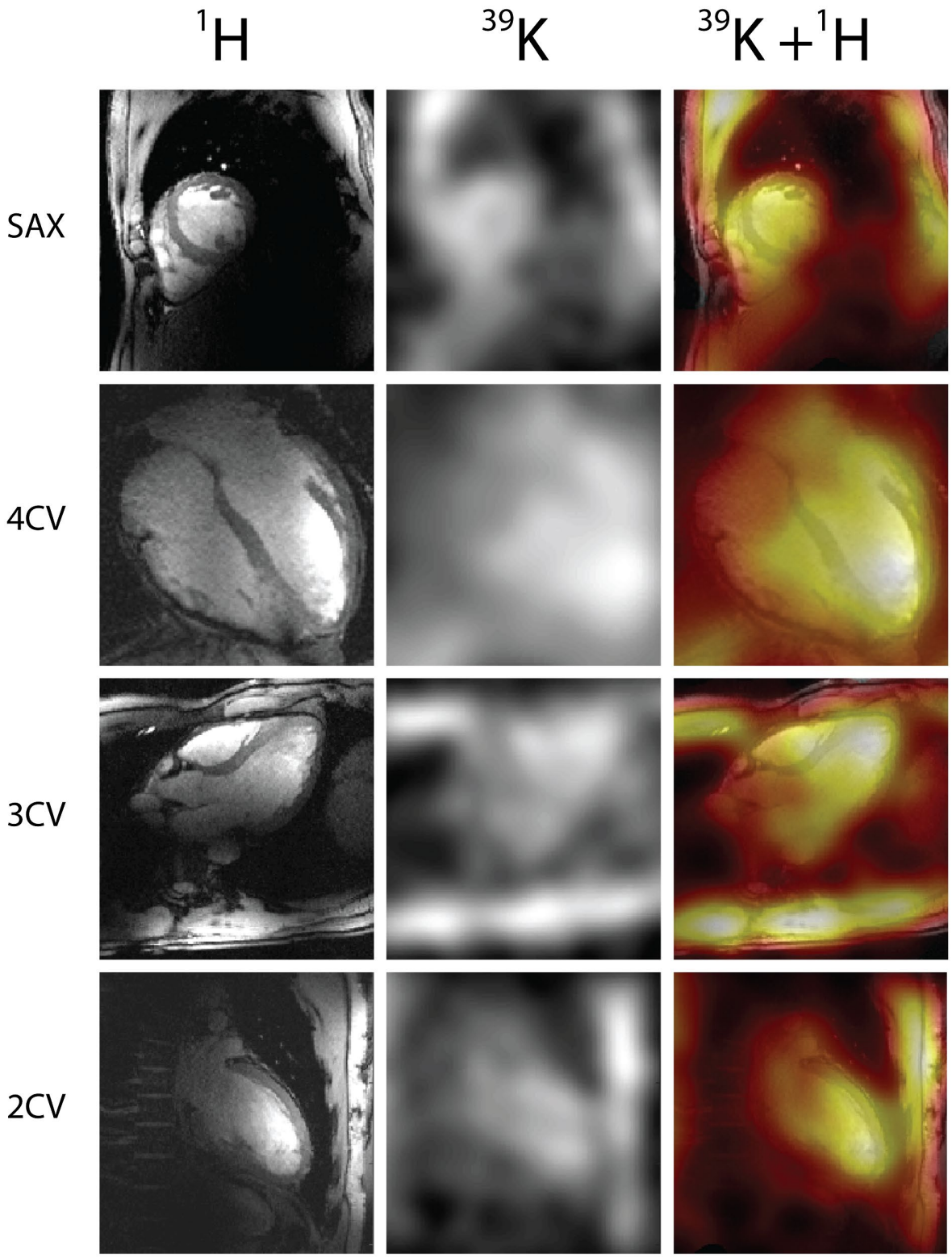

FIGURE 6 Left column: ^{1}H images of the heart obtained from a healthy male volunteer (age = 27 years; BMI = 27.1 kg/m^{2}) by using following parameters: TE/TR = 2.67/5.66 ms, FOV = (360 × 291) mm^{2}, in-plane resolution = (1.4 × 1.4) mm^{2}, slice thickness = 4.0 mm, flip angle = 32°, acquisition time = 12 s. Middle column: in vivo ^{39}K images of the same volunteer obtained using DA-3DPR imaging; filtered with Hamming filter and four-time zero filling and demonstrated in short axis (SAX), four-chamber (4CV), 3-chamber (3CV) and 2-chamber (2CV) view. The images were acquired with nominal isotropic resolution = 14.5 × 14.5 × 14.5 mm^{3} within 30 min by using following parameters: TR/TE = 30/0.7 ms, number of projections = 20,000, readout duration = 5 ms. Right column: overlay of ^{39}K and ^{1}H images

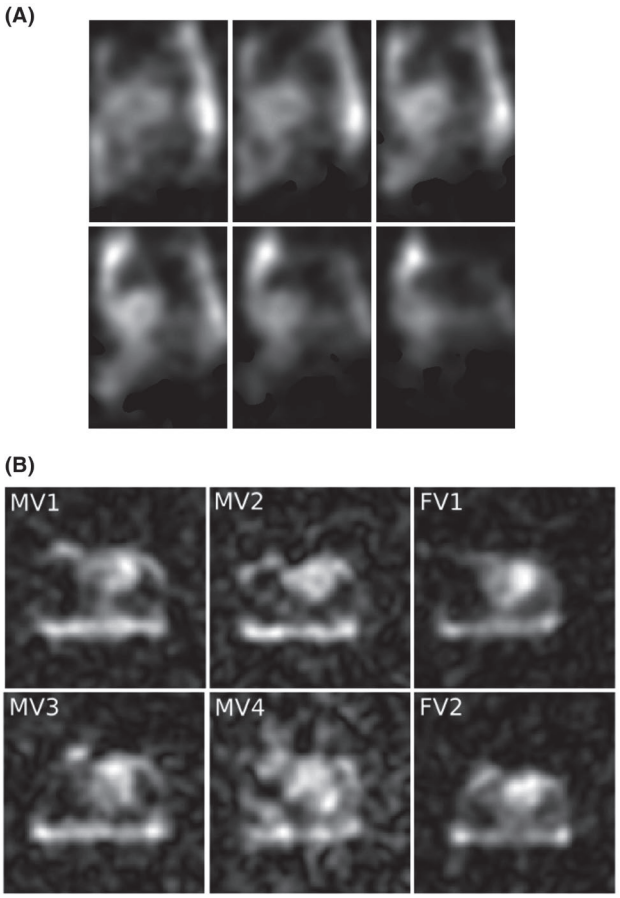

FIGURE 7 (A) Six slices of in vivo ^{39}K images of the same volunteer as in Figure 6 obtained using DA-3DPR imaging; filtered with Hamming filter and four-time zero filling and demonstrated in short axis (SAX) view. The images were acquired with nominal isotropic resolution = 14.5 × 14.5 × 14.5 mm^3 within 30 min by using following parameters: TR/TE = 30/0.7 ms, number of projections = 20,000, readout duration = 5 ms. (B) In vivo ^{39}K MR images, shown in axial view, obtained from 6 healthy volunteers: 4 male (MV1, MV2, MV3, MV4) and 2 female (FV1, FV2) using the same imaging technique as in Figure 6, but different MR system (Terra, Siemens Healthineers, Erlangen, Germany)

such a low resonant frequency.[19] The RF coil proposed here supports potassium and proton imaging of the human heart at 7.0T. At the resonance frequency of ^{1}H at 7.0T, conductors, which are typical for the resonance frequency of ^{39}K at 7.0T, would be too long and might act as antennas, causing undesired RF interactions between the ^{39}K and ^{1}H coils. This makes the potential use of multiple-turn coils questionable.

Potassium ions are crucial for life and their significance for cardiac physiology and metabolism extends beyond the function they play in the activity of Na^+/K^+-ATPase. The links between molecular mechanisms involving K^+ channels expressed in human heart and higher risk of arrhythmias remain poorly understood.[6] Pathologic alterations in K^+ concentration have profound implications in a number of cardiovascular contexts, underscoring the broad roles of this element in processes related to heart physiology.

In vivo ^{39}K MRI offers an interesting alternative approach to explore tissue-specific pathophysiological changes that can complement ^{23}Na MRI-based techniques. The accuracy of the methods currently used to distinguish between extracellular and intracellular sodium remains controversial. Nevertheless, ^{39}K MRI is highly promising, because the physio-metabolic information it could provide can be associated almost exclusively with intracellular space.

Undoubtedly, the future of ^{39}K MRI of the heart will not end at 7.0T, and the field is moving apace in this direction. Electrolyte mapping is one of the key applications desired by the community of scientists and clinicians who are advocating for 14.0T and 20.0T human MR scanners,[20,21] as outlined in a report of the National Research Council on high magnetic field science and its application.[22] This report forwarded a call for a 20.0T wide bore MR system—a technical development inspired by the recent progress at 7.0T. The sensitivity gain at 20.0T is expected to reduce scan times for ^{39}K MRI by a factor of 8, compared to the 7.0T capabilities available today. Although this remains, for the moment, merely a vision, it promises potassium MR with an isotropic spatial resolution of 8 mm (assuming a linear noise model) achievable within the same scan time used in our study. Together with other relevant nuclei such as ^{23}Na and ^{35}Cl, this will provide new opportunities for ^{39}K MRI to drive the exploration of structures, functions and physio-metabolic processes of the human heart.

ACKNOWLEDGMENTS

This work was funded by the Helmholtz Alliance iMED, the Helmholtz Initiative on Personalized Medicine. The authors wish to acknowledge Antje Els (Max Delbrueck Center for Molecular Medicine, Berlin, Germany) for help with ^{1}H CMR data acquisition; Jason Millward (Max Delbrueck Center for Molecular Medicine, Berlin, Germany) for his feedback on the manuscript; and Darius Lysiak, Helmar Waiczies (MRI.TOOLS GmbH, Berlin, Germany) who provided the Plexiglas shell of the torso phantom. The authors are also grateful for the help provided by Reiner Umathum, Nico Behl, and Arthur Magill (German Cancer Research Center, Heidelberg, Germany) who supported the ^{39}K cardiac MRI sessions. This fruitful collaboration resulted in the first ^{39}K image that was presented at the ISMRM workshop on "MR Imaging of nX-Nuclei (23Na & Friends): From Controversies to Potential Clinical Applications" that took place in Dubrovnik, Croatia, April 7–10, 2018 (https://www.ismrm.org/workshops/2018/XNuclei/). We also acknowledge Ignacio Gonzalez Insua, Markus Adriany (Siemens Healthineers) and Helmut Stark (Stark Contrast) for technical support during our in vivo experiments in Erlangen.

CONFLICT OF INTEREST

Andre Kuehne is employee of MRI.TOOLS GmbH, Berlin, Germany. Thoralf Niendorf is founder and CEO of MRI. TOOLS GmbH, Berlin, Germany.

ORCID

Daniel Wenz https://orcid.org/0000-0002-3216-7599

REFERENCES

1. Doyle DA, Morais Cabral J, Pfuetzner RA, et al. The structure of the potassium channel: molecular basis of K+ conduction and selectivity. *Science*. 1998;280:69–77.
2. Skou JC. The influence of some cations on an adenosine triphosphatase from peripheral nerves. *Biochim Biophys Acta*. 1957;23:394–401.
3. Carmeliet E. Cardiac ionic currents and acute ischemia: from channels to arrhythmias. *Physiol Rev*. 1999;79:917–1017.
4. Deal KK, England SK, Tamkun MM. Molecular physiology of cardiac potassium channels. *Physiol Rev*. 1996;76:49–67.
5. Parrish TB, Fieno DS, Fitzgerald SW, Judd RM. Theoretical basis for sodium and potassium MRI of the human heart at 1.5 T. *Magn Reson Med*. 1997;38:653–661.
6. Giudicessi JR, Ackerman MJ. Potassium-channel mutations and cardiac arrhythmias–diagnosis and therapy. *Nat Rev Cardiol*. 2012;9:319–332.
7. Fieno DS, Kim RJ, Rehwald WG, Judd RM. Physiological basis for potassium (39K) magnetic resonance imaging of the heart. *Circ Res*. 1999;84:913–920.
8. Nelson MT, Quayle JM. Physiological roles and properties of potassium channels in arterial smooth muscle. *Am J Physiol*. 1995;268(4Pt1):C799–822.
9. International Electrotechnical Commision. Medical electrical equipment. Part 2–33: particular requirements for the safety of magnetic resonance equipment for medical diagnosis. Volume 60601-2-33, Edition 3. Geneva: International Electrotechnical Commission. 2010. 219 p.
10. Christ A, Kainz W, Hahn EG, et al. The virtual family–development of surface-based anatomical models of two adults and two children for dosimetric simulations. *Phys Med Biol*. 2010;55:N23–38.
11. Hasgall PA, Di Gennaro F, Baumgartner C, et al. *IT'IS Database for thermal and electromagnetic parameters of biological tissues*. Version 4.0. 2018. https://doi.org/10.13099/VIP21000-04-0. Accessed August 19, 2019.
12. Nagel AM, Laun FB, Weber MA, Matthies C, Semmler W, Schad LR. Sodium MRI using a density-adapted 3D radial acquisition technique. *Magn Reson Med*. 2009;62:1565–1573.
13. Umathum R, Rosler MB, Nagel AM. In vivo 39K MR imaging of human muscle and brain. *Radiology*. 2013;269:569–576.
14. Shinar H, Eliav U, Navon G. Single and multiple quantum NMR relaxation times of sodium and potassium in red blood cells. *Isr J Chem*. 1992;32:299–304.
15. Rosler MB, Nagel AM, Umathum R, Bachert P, Benkhedah N. In vivo observation of quadrupolar splitting in (39)K magnetic resonance spectroscopy of human muscle tissue. *NMR Biomed*. 2016;29:451–457.
16. Hald PM. Notes on the determination and distribution of sodium and potassium in cells and serum of normal human blood. *J Biol Chem*. 1946;163:429–434.
17. De Zanche N, Yahya A, Vermeulen FE, Allen PS. Analytical approach to noncircular section birdcage coil design: verification with a Cassinian oval coil. *Magn Reson Med*. 2005;53:201–211.
18. Platt T, Umathum R, Fiedler TM, et al. In vivo self-gated (23) Na MRI at 7 T using an oval-shaped body resonator. *Magn Reson Med*. 2018;80:1005–1019.
19. Blasiak B, Volotovskyy V, Deng C, Tomanek B. An optimized solenoidal head radiofrequency coil for low-field magnetic resonance imaging. *Magn Reson Imaging*. 2009;27:1302–1308.
20. Niendorf T, Paul K, Oezerdem C, et al. W(h)ither human cardiac and body magnetic resonance at ultrahigh fields? technical advances, practical considerations, applications, and clinical opportunities. *NMR Biomed*. 2016;29:1173–1197.
21. Niendorf T, Schulz-Menger J, Paul K, Huelnhagen T, Ferrari VA, Hodge R. High field cardiac magnetic resonance imaging: a case for ultrahigh field cardiac magnetic resonance. *Circ Cardiovasc Imaging*. 2017;10:e005460.
22. National Research Council. *High Magnetic Field Science and Its Application in the United States: Current Status and Future Directions*. Washington, DC: The National Academies Press; 2013. https://doi.org/10.17226/18355.

How to cite this article: Wenz D, Nagel AM, Lott J, Kuehne A, Niesporek SC, Niendorf T. In vivo potassium MRI of the human heart. *Magn Reson Med*. 2020;83:203–213. https://doi.org/10.1002/mrm.27951